Tectonophysics 666 (2016) 158–163

Contents lists available at ScienceDirect

Tectonophysics

journal homepage: www.elsevier.com/locate/tecto

Evolution of the internal structure of fault zones in three-dimensional numerical models of normal faults

Martin P.J. Schöpfer *, Conrad Childs, John J. Walsh, Tom Manzocchi

Fault Analysis Group, UCD School of Earth Sciences, Belfield, Dublin 4, Ireland

ARTICLE INFO

Article history:
Received 2 February 2015
Received in revised form 3 November 2015
Accepted 5 November 2015
Available online 12 November 2015

Keywords:
Fault zone structure
Fault lenses
Asperity bifurcation
Tip-line bifurcation
Distinct element method

ABSTRACT

Fault zone internal structure is characterised by heterogeneous distributions of both continuous (drag, lens rotation) and discontinuous (joints, faults) deformation which cannot be easily modelled using continuum numerical methods. Distinct element method (DEM) models, that exhibit bulk rheologies comparable to rock, demonstrate emergent behaviours that make them ideal for modelling both the nucleation and growth of fault zones. The ability to model fault zones numerically allows extant conceptual models for fault zone evolution based on outcrop studies to be tested, and controls on fault zone structure to be analysed. Three-dimensional DEM models of faults zones in mechanically layered sequences demonstrate that internal fault zone structure is predominantly controlled by the geometry of the initial fault. Whether the initial fault is a segmented array or an irregular surface determines the complexity of structure it will develop as displacement increases. Confining pressure at the time of faulting determines the irregularity of the initial fault array and also the efficiency with which irregularities are incorporated into a fault and subsequently comminuted, leading to a relationship whereby brittle faulting at high confining pressure results in less complex internal fault zone structure than at low confining pressure.

1. Introduction

Recent studies of fault zones have tended to concentrate on characterisation of a central zone of high strain (fault core) and an enveloping zone of low strain (damage zone; e.g. Caine et al., 1996; Faulkner et al., 2003; Shipton and Cowie, 2003; Kim et al., 2004). However fault zones often display a more complex structure with displacement distributed onto anastomosing slip surfaces or zones of intense deformation (Wallace and Morris, 1986; Cox and Scholz, 1988; Faulkner et al., 2003; Fig. 1). Relatively few studies have addressed this more complex strain distribution or have attempted to quantify how displacement is partitioned onto different slip surfaces (e.g. Ferrill et al., 2011). These considerations are of significant practical importance in application areas concerned with across-fault connectivity (e.g. trapping of hydrocarbons), but are also important in understanding fault zone growth, because displacement partitioning records a critical aspect of the geometrical evolution of fault zones.

The development of complex internal fault zone structure has been attributed to the repeated action of two processes, (i) shearing-off of fault surface irregularities by the formation of a new slip surface and (ii) linkage between initially unconnected segments of a fault array to enclose the intervening rock volume (referred to as asperity and tip-line bifurcation, respectively; Childs et al., 1996). These processes have been invoked from the study of outcrops and seismic reflection data (Childs et al., 2009; Peacock and Sanderson, 1991; Walsh et al., 2003) and underpin a geometric model of fault zone evolution in which fault zone structure is strongly controlled by initial fault geometry (Childs et al., 2009). While the action of these processes is supported by observations from laboratory analogue experiments (e.g., Fossen and Gabrielsen, 1996), numerical modelling is better suited to systematically investigate the impact of lithology, deformation conditions and scale on the evolution of fault zone structure (Mandl, 2000).

The primary aim of this paper is to show that, in carefully designed 3D numerical models of fault zone evolution, complex fault zone structure develops by tip-line and asperity bifurcation processes and that these arise because of segmentation and irregularity of the fault when it first propagates through the model volume. We use a discontinuum numerical approach, the 3D distinct element method (DEM), to model the evolution of normal fault zones in mechanically layered sequences (equivalent 2D models were previously described by Schöpfer et al., 2006, 2007a,b, 2009a). The distinct element method is ideal for this purpose as it can model both the nucleation of fractures/faults and the accumulation of large heterogeneous strains (Cundall, 2001). Of the various factors that control fault zone evolutionary processes in these models we illustrate the effect of confining pressure.

2. Distinct element method numerical modelling

We use the particle flow code in three dimensions (PFC-3D; Itasca Consulting Group, 2008), which implements the DEM for spherical

* Corresponding author at: Department for Geodynamics and Sedimentology, University of Vienna, Althanstrasse 14, A-1090 Vienna, Austria. Tel.: +43 1 4277 53363.
E-mail address: martin.schoepfer@univie.ac.at (M.P.J. Schöpfer).

http://dx.doi.org/10.1016/j.tecto.2015.11.003
0040-1951/

Fig. 1. Fault with a displacement of 11 m offsetting a limestone sequence at Il-Blata, SW Malta (Photo: C.G. Bonson). The fault surface dips steeply to the right and the upper surface of the limestone bed in the footwall and hanging wall are labelled. Arrows indicate the displacement of a lens within the fault zone and a lens of limestone breccia is also labelled (L). The cuspate shape of the footwall cut-off and irregularity of the fault surface is attributed to excision of limestone lenses, possibly the result of fault dip refraction (the much weaker Globigerina Limestone overlying the massive Lower Coralline limestone pictured here has been eroded).

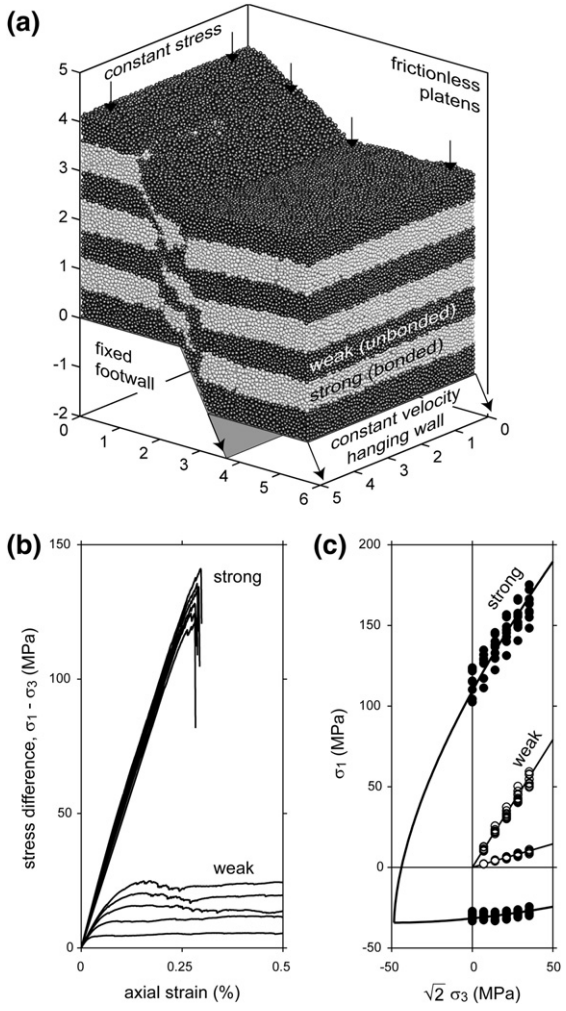

Fig. 2. DEM modelling of fault growth in a multilayer sequence. (a), PFC3D model (scale in metres) illustrating the model boundary conditions (see text). The layers in this particular model are 0.6 m thick. (b), Stress–strain curves for confining pressures of 0, 5, 10, 15, 20 and 25 MPa of the strong and weak materials used in the model shown in (a) (and in Fig. 4; see Table 1). (c), Best-fit failure criteria drawn through the peak-stress data on the triaxial plane graph are the Lade–Duncan criterion and non-linear Lade criterion with cohesion (Lade, 1997), for the weak (open circles) and strong materials (black circles), respectively. These are referred to in text as shale and sandstone.

particles that interact with each other via linear elastic and frictional (Coulomb) contact laws and can be bonded together with a linear elastic 'cement' that breaks if its strength is exceeded (Potyondy and Cundall, 2004). Each fault zone model contains ~250,000 particles representing a $5 \times 5 \times 4$ m rock volume comprising interbeds of strong (bonded particles) and weak (non-bonded particles) layers (Fig. 2a). At the scale of the modelled volume the effects of gravity are negligible and models are run without gravitational acceleration so that the results are most applicable at the outcrop scale. At significantly larger scales body forces due to gravity may alter the emergent fault geometries and processes.

The particles have a uniform size distribution with radii between 0.05 m and 0.03 m. It is worthwhile emphasising that the spherical elements and the bonds between them are a means of discretising the model and do not necessarily represent grains in a natural rock or cement. The bulk mechanical behaviour of a model material emerges from the interaction of particles via bonds and their contacts so that different combinations of microproperties of particles and bonds yield model materials with different macroproperties (Table 1). The macroscopic response cannot be predicted analytically for randomly packed polydisperse spheres and therefore was determined in numerical laboratory tests (Fig. 2b and c), and calibrated to the behaviours of natural rocks (Schöpfer et al., 2009b). The weak materials exhibit linear pressure-dependence (Fig. 2c) with bulk friction coefficients of 0.40–0.48, have no tensile strength and are comparable with weak sedimentary rocks such as shales or mudrocks. The strong materials exhibit complex, non-linear pressure dependent behaviour (Fig. 2c) with a variety of macroproperties, (e.g. Young's modulus and unconfined compressive strength, see Table 1 for details), which are comparable to those of strong sedimentary rocks such as sandstones. Although some

Table 1
Mechanical properties of 'sandstone' layers used in faulting models.

Figure number	Layer thickness[c]	Microproperties[a]		Macroproperties[b]	
		$E_c = \bar{E}_c$	$\overline{\sigma}_c = \overline{\tau}_c$	E	UCS[d]
	(m)	(GPa)	(MPa)	(GPa)	(MPa)
3	0.60	25	50 ± 10	20.4 ± 0.8	50.8 ± 4.6
4	0.60	50	100 ± 20	39.8 ± 1.0	100.0 ± 7.8
5	0.45	50	100 ± 20	36.9 ± 1.9	87.8 ± 12.5

[a] Contact and bond modulus, $E_c = \bar{E}_c$, are constant in each model. Particles comprising 'sandstone' layers are bonded with equal tensile and shear strength, $\overline{\sigma}_c = \overline{\tau}_c$, drawn from a normal distribution (plus/minus one standard deviation given). Microproperties that are not varied in this study are contact friction coefficient, $\mu_c = 0.5$, contact and bond normal to shear stiffness ratio, $k_n / k_s = \bar{k}_n / \bar{k}_s = 2.5$, and the bond width multiplier, $\lambda = 1$. Definition of these microproperties and modulus–stiffness scaling relations are given in Potyondy and Cundall (2004).

[b] Numerical rock properties obtained from ten unconfined compression tests are given as mean plus/minus one standard deviation. E, Young's modulus; UCS, unconfined compressive strength.

[c] The sandstone and interbedded shale layers have always the same thickness. The shale layers have always identical particle properties to the sandstone layers but are unbonded (cohesionless).

[d] The ratio of unconfined compressive strength (UCS) to unconfined tensile strength (UCT) is ~3.5.